Am J Cancer Res 2015;5(11):3485-3504
www.ajcr.us /ISSN:2156-6976/ajcr0014702

Original Article

Mediated coalescence: a possible mechanism for tumor cellular heterogeneity

Joseph Ambrose, Michelle Livitz, Deborah Wessels, Spencer Kuhl, Daniel F Lusche, Amanda Scherer, Edward Voss, David R Soll

Developmental Studies Hybridoma Bank, Department of Biology, University of Iowa, Iowa City, Iowa 52242, USA

Received August 18, 2015; Accepted September 18, 2015; Epub October 15, 2015; Published November 1, 2015

Abstract: Recently, we demonstrated that tumorigenic cell lines and fresh tumor cells seeded in a 3D Matrigel model, first grow as clonal islands (primary aggregates), then coalesce through the formation and contraction of cellular cables. Non-tumorigenic cell lines and cells from normal tissue form clonal islands, but do not form cables or coalesce. Here we show that as little as 5% tumorigenic cells will actively mediate coalescence between primary aggregates of majority non-tumorigenic or non-cancerous cells, by forming cellular cables between them. We suggest that this newly discovered, specialized characteristic of tumorigenic cells may explain, at least in part, why tumors contain primarily non-tumorigenic cells.

Keywords: Intra-tumor heterogeneity, field effect, cancer cell motility, 4D reconstruction, tumor cell contact, aggregate coalescence

Introduction

When cells from a variety of different tumors are dissociated, a surprisingly high proportion proves to be non-tumorigenic [1-4]. Moreover, the cells within a tumor can be diverse both phenotypically [5-7] and genotypically [8, 9]. A major supposition is that tumors arise clonally and therefore phenotypic heterogeneity is developmental. Cells in a tumor differentiate in space and time, and the minority that are tumorigenic have retained an undifferentiated and hence tumorigenic phenotype [1]. This has provided part of the basis for the cancer stem cell theory [10, 11]. However, there is another theory, the field cancerization effect [12], first put forth by Slaughter et al. [13]. He based this theory on a high incidence of multiple primary tumors observed in case studies of head and neck cell carcinomas [13]. He suggested that tumor growth could be mediated, at least in part, by the coalescence of multiple tumorigenic foci within a tissue, a process that would contribute to tumor heterogeneity. Subsequently, field cancerization has been described in many other cancers [14-22].

Recently, we developed a computer-assisted *in vitro* model for reconstructing in 3D cell behavior in a 3D Matrigel matrix over extended periods of time [23-25]. Imaging is accomplished using differential interference contrast microscopy (DIC) and, therefore, does not require dyes or fluorescent techniques, which introduce toxicity [26, 27]. A single z-series through 1 mm of Matrigel can be acquired at time intervals as short as once every 5 seconds and the process repeated indefinitely. Using this model, we discovered that cells from tumorigenic cell lines and fresh tumors, when seeded in a 3D Matrigel matrix, grow into clonal islands, or primary aggregates, that then coalesce to form large aggregates. These large aggregates then undergo morphogenesis to generate a highly structured, large spherule [23-25]. Coalescence is facilitated by specialized cells that exit neighboring aggregates, forming cellular cables between the primary aggregate. These cables contract, moving smaller aggregates into larger ones. This active process continues, generating a final large aggregate that then undergoes differentiation. We found this general scenario true for cells from tumor tissues and cell line from a variety of cancers. In marked contrast, non-tumorigenic, or very weakly tumorigenic lines, and cells from healthy control tissues, also form clonal islands in a 3D Matrigel through cell multiplication, but then fail to gen-

erate the specialized cells and fail to undergo coalescence [24].

Here, we have investigated the possibility that tumor heterogeneity, most notably mixtures of majority non-tumorigenic cells and minority tumorigenic cells, may be due not only to the differentiation of cells within a tumor, but also to the active recruitment of non-tumorigenic cells by tumorigenic cells into the tumor. To investigate this hypothesis, we have employed the tumorigenic breast cancer cell line, MoVi-10´, which was engineered through overexpression of the intermediate filament vimentin, and either the weakly tumorigenic parent line, MCF-7 or the non-tumorigenic breast cell line MCF-10A [28], both of which do not undergo coalescence [29]. We show that as little as 5% of tumorigenic MoVi-10´ cells will actively cause primary aggregates of majority MCF-7 cells or MCF-10A cells, formed by cell multiplication, to undergo coalescence. Using differential expression of GFP, we further demonstrate that coalescence is mediated by the formation of cables composed entirely of minority MoVi-10´ cells. These cellular cables contract, pulling smaller aggregates of non-tumorigenic cells into larger aggregates. These results suggest an alternative mechanism for the presence of a high percentage of non-tumorigenic cells within a given tumor and thus provide an additional perspective on how tumor heterogeneity may arise *in vivo*.

Methods

Cell culture

The weakly tumorigenic, parental breast cancer cell line MCF-7 and its tumorigenic, vimentin over-expressing derivative MoVi-10´ were generous gifts from Dr. Mary Hendrix (Northwestern University Feinberg School of Medicine) [29]. MoVi-10´ and MCF-7 cells were cultured in RPMI medium (RPMI 1640, Life Technologies, Carlsbad, CA) supplemented with 10% (v/v) heat-inactivated fetal bovine serum (Atlanta Biologicals, Norcross, GA), 1X GlutaMAX (Life Technologies) and penicillin/streptomycin (Life Technologies). A GFP-tagged MCF-7 cell line was obtained from Cell Biolabs (San Diego, CA; http://www.cellbiolabs.com) and cultured in Dulbecco's Modified Eagle's medium (DMEM, Life Technologies, Carlsbad, CA) supplemented with 10% FBS and 1X nonessential amino acids (Life Technologies, Carlsbad, CA). MCF-10A, a non-tumorigenic cell line, derived from normal breast epithelial cells [28], was obtained from the American Type Culture Collection (http://www.atcc.org) and maintained in mammary epithelial cell basal medium supplemented with epidermal growth factor, hydrocortisone, insulin (MEGM Bullet Kit, Lonza) and cholera toxin (100 ng/ml, Sigma) [30]. MDA-MB-231 cells were obtained from Sigma-Aldrich (http://www.sigmaaldrich.com) and cultured in L-15 medium supplemented with 15% fetal bovine serum (Atlanta Biologicals, Norcross, GA), 1X GlutaMAX (Life Technologies, Carlsbad, CA) and penicillin/streptomycin (Life Technologies, Carlsbad, CA). The inflammatory breast cancer cell line SUM149 was a generous gift from Dr. Kenneth Van Golen (University of Delaware, Newark, DE). SUM149 cells were cultured in Ham's F-12 medium supplemented with 5% fetal bovine serum, penicillin/streptomycin (Life Technologies), 1X GlutaMAX (Life Technologies), 10 μg/mL insulin, 5.5 μg/mL transferrin, 6.7 ng/mL selenium (Thermofisher, www.thermofisher.com), and 1 μg/mL hydrocortisone (Thermofisher, www.thermofisher.com). The tumorigenic line MDA-MB-435-α6HG6 [31, 32], a generous gift from Dr. Suranganie Dharmawardhane of the University of Puerto Rico School of Medicine, San Juan, Puerto Rico, was cultured as previously described [24]. Cells were passaged using standard culture techniques. For experimentation, cells from all lines were harvested at approximately 70% confluency.

2D analysis of cell motility

An aliquot of the reconstituted basement membrane matrix Matrigel (Corning Life Science, Corning, NJ) was thawed on ice and handled with ice-cold pipette tips according to the manufacturer's instructions. As previously described, [24] the 20 mm glass insert of a 30 mm plastic petri dish (Cellvis; www.cellvis.com) was first coated with 500 μl of chilled Matrigel and incubated for 30 minutes at 37°C to allow gelation. Cells were harvested and plated onto the pre-coated dish at a density of 1×10^4 cells in 100 μl of cell culture media and incubated for 30 minutes to allow the cells to attach before filling the dish with media. The covered dish was then placed on the stage of a microscope positioned within an incubator set to 37°C and

5% CO_2. A time series of JPEG images was acquired using brightfield optics and a 10X objective at 2 minute intervals with Fire-I software (http://fire-i-application.software.informer.com). The JPEG files were assembled sequentially into a 2D movie using J3D-DIAS 4.1 software. Automatic outlining of single cells, generation of paths and data calculations were performed as described elsewhere [25, 33-37].

2D analysis of coalescence

A 30 mm glass insert of a 60 mm dish was coated with 300 µl of Matrigel [24]. The Matrigel coat was allowed to gel by incubation for 30 minutes at 37°C. MoVi-10´ and MCF-7 cells were harvested and either used homogeneously, or MCF-7 cells were mixed with MoVi-10´ cells in different preparations. Unmixed and mixed cultures, all containing a total of 5×10^5 cells suspended in 300 µl of media, were spread onto the Matrigel coated glass insert and allowed to attach for 30 minutes. Chilled cell culture media supplemented with 5% Matrigel was then added to the dish, coating the cells in a thin layer of Matrigel [38]. The culture was placed on the stage of a microscope housed in 5% CO_2 incubator and incubated at 37°C undisturbed for 30 minutes. Coalescence was then monitored by acquiring JPEG images through a 4X or 10X objective in 2D, and the number of aggregates assessed at 0 and 72 hours. Relative coalescence was computed as the number of cells at 0 hours minus the number of aggregates at 72 hours, divided by the number of cells at 0 hours. To determine if a minority of MoVi-10´ cells induced aggregation in a majority population of the non-tumorigenic MCF-10A cells, MoVi-10´ cells were first adapted to MCF-10A media. Adaptation was accomplished by initially transferring cells into media consisting of 50% of the MoVi-10´ medium, as described above, and 50% of the MCF-10A medium also as described above. At the next passage, cells were transferred into 100% of the MCF-10A media [23]. After the adaptation period, cultures containing 10% MoVi-10´ cells and 90% MCF-10A cells were prepared, as described above for mixed cultures of MoVi-10´ and MCF-7. To determine if MoVi-10´ cells formed bridges between islands of MCF-10A cells in mixed cultures, MoVi-10´ cells were mixed with 90% GFP-tagged MCF-7 cells as described above and incubated for 24 hrs.

3D cell culture

Cells were cultured in a 3D Matrigel as previously described in detail [24]. In brief, 100 µl of Matrigel was spread onto the 30 mm diameter glass insert of a 60 mm dish (Cellvis; www.cellvis.com) that was modified for DIC imaging as described in Scherer et al. [24]. The Matrigel coat was allowed to gel for 20 minutes at 37°C. Cells were harvested from growth flasks prior to confluency, diluted to a density of 5×10^6 cells per ml in 250 µl of culture media, gently mixed, chilled and then added to 500 µl of ice cold Matrigel. The entire mixture was plated atop the base layer and allowed to gel for 30 minutes at 37°C. The appropriate medium was then added to the dish and gently replaced at three day intervals over the course of the experiment. Aggregation behavior was recorded using a 3D microscope housed in a 37°C, 5% CO_2 incubator with 90% humidity, described at length in Scherer et al. [24], and analyzed using J3D-DIAS 4.1, summarized below and described elsewhere in detail [23-25].

3D image acquisition and optical sectioning

3D cultures of cells embedded in Matrigel were placed on the stage of a Zeiss Axioplan 2 microscope equipped with differential interference contrast (DIC) optics, a motor-driven stage, and a Zeiss AxioCam MRc5 IEEE 1394 color CCD camera, all of which were housed within an incubator set at 37°C and 5% CO_2 as described elsewhere in considerable detail [23-25]. In brief, optical sectioning was performed at 10 µm increments using a 20X objective. In this manner, a z-series of 150 high resolution, moderately compressed JPEG images was acquired once every 30 minutes for up to 8 days. The entire series over time was then saved in movie format in J3D-DIAS 4.1, for subsequent object detection, 4D reconstruction, path generation and motion analysis.

J3D-DIAS 4.1 object detection, 4D reconstruction, path generation and data calculation

J3D-DIAS 4.1 automatically detected the in-focus regions of cells and aggregates in each optical section using the "complexity-based bitmap object detection" (C-BBOD) algorithm described elsewhere in detail [24, 25]. Overlapping traces in each z-series were then stacked to generate discrete objects in 4D. The

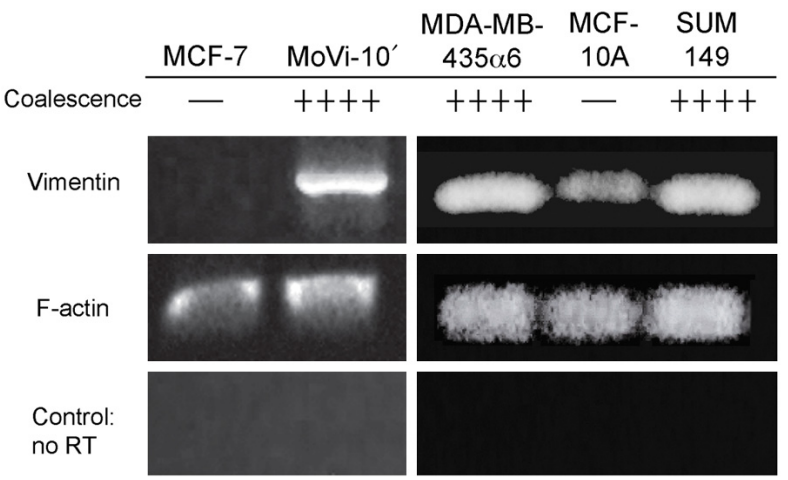

Figure 1. Vimentin is up-regulated in MoVi-10´. The levels of vimentin transcript were assessed by reverse transcription polymerase chain reaction (RT-PCR). RT-PCR analysis of vimentin reveals neglible expression in MCF-7 and a high level of expression in MoVi-10´ cells. RT-PCR analysis of vimentin expression reveals a high level of expression in in MDA-MB-435-α6HG6 and SUM149 cells and a reduced level in MCF-10A. The F-actin transcript was used to verify uniform loading. The control represents preparations in which reverse transcriptase was omitted.

"adaptive skeleton climbing isoform extraction" algorithm [24, 25, 39] was then applied to each object to generate a wrapped, faceted surface. Irregularities in the 4D reconstruction were attenuated by vertex smoothing [40]. The 3D centroid of each object in each frame was determined from the x, y and z coordinates of its center and the centroids connected over time to generate the 4D centroid path [33-35, 41-44]. Instantaneous velocities of cells and aggregates were calculated from the position of the 4D centroid path using the central difference method [45]. This method, in effect, smooths out extreme variations or noise at each centroid position [33]. At each frame or time point (n), the centroid position of the reconstructed cell or aggregate is determined from its x-, y-, and z-coordinates. A vector is drawn from the centroid in frame n-1 to the centroid position in frame n+1, and the length of the vector dived by twice the time interval between the two time points [33]. Surface complexity was calculated from the formula $1/(6 \sqrt{\pi} \text{Vol}/(\text{surface area}^{3/2}))$, where Vol is volume and *sqrt* is the square root. Coalescence was quantified by the "field density" parameter, derived by drawing the smallest possible cube around all objects in the field in each frame and determining the volume of all objects contained within the cube as well as the volume of the cube itself. The ratio of the sum of the object volumes over the volume of the cube was calculated and multiplied by 100 to obtain the field density [23-25].

Reverse transcriptase-polymerase chain reaction

RT-PCR was performed as previously described [46]. In brief, RNA was isolated using Trizol (Life technologies, Carlsbad, CA) as described by the manufacturer. 1 μg of total RNA was treated with Dnase I (Ambion, Life Technologies, Carlsbad, CA) according to the manufacturer's instruction to remove residual genomic DNA. For reverse transcription, the Omniscript RT-PCR Kit (Qiagen, Ventura, CA) was used. The RNA was pretreated at 65°C for 5 min, underwent reverse transcription in a total volume of 20 μl using the OligodT primer supplied by the manufacturer. The resulting cDNA was amplified using the Long Range Expand Polymerase Kit (Roche, Indianapolis, IN). 500 ng of total cDNA was used as a template for the primer Vimentin FW 5'-ATGTCTACCAGGTCTGTGTCCTCGTCCTCCTACCGCAGGATGTTC-3' and Vimentin RV 5'-TTATTCAAGGTCATCGTGATGCTGAGAAGTCTCATTGATCACCTGTCC-3', to amplify a 1.4 KB vimentin cDNA. To ensure equal loading, human β-actin was amplified from 10 ng total cDNA of each strain using the primers ActinFW 5'-CATGTACGTTGCTATCCAGGC-3' and ActinRV 5'-CTCCTTAATGTCACGCACGAT-3', resulting in a 229 Bp fragment.

Light and fluorescence microscopy

Preparations containing GFP-tagged MCF-7 cells were imaged in parallel with DIC optics and fluorescence optics, using a 20X objective on a Nikon TE2000 inverted fluorescence microscope (Nikon Instruments, Melville, NY) connected to a Bio-Rad RadianceMP 2100 laser scanning confocal microscope.

Results

2D-DIAS analysis of single cell behavior

MoVi-10´ [29] was derived from the cell line MCF-7, a weakly tumorigenic breast cancer cell

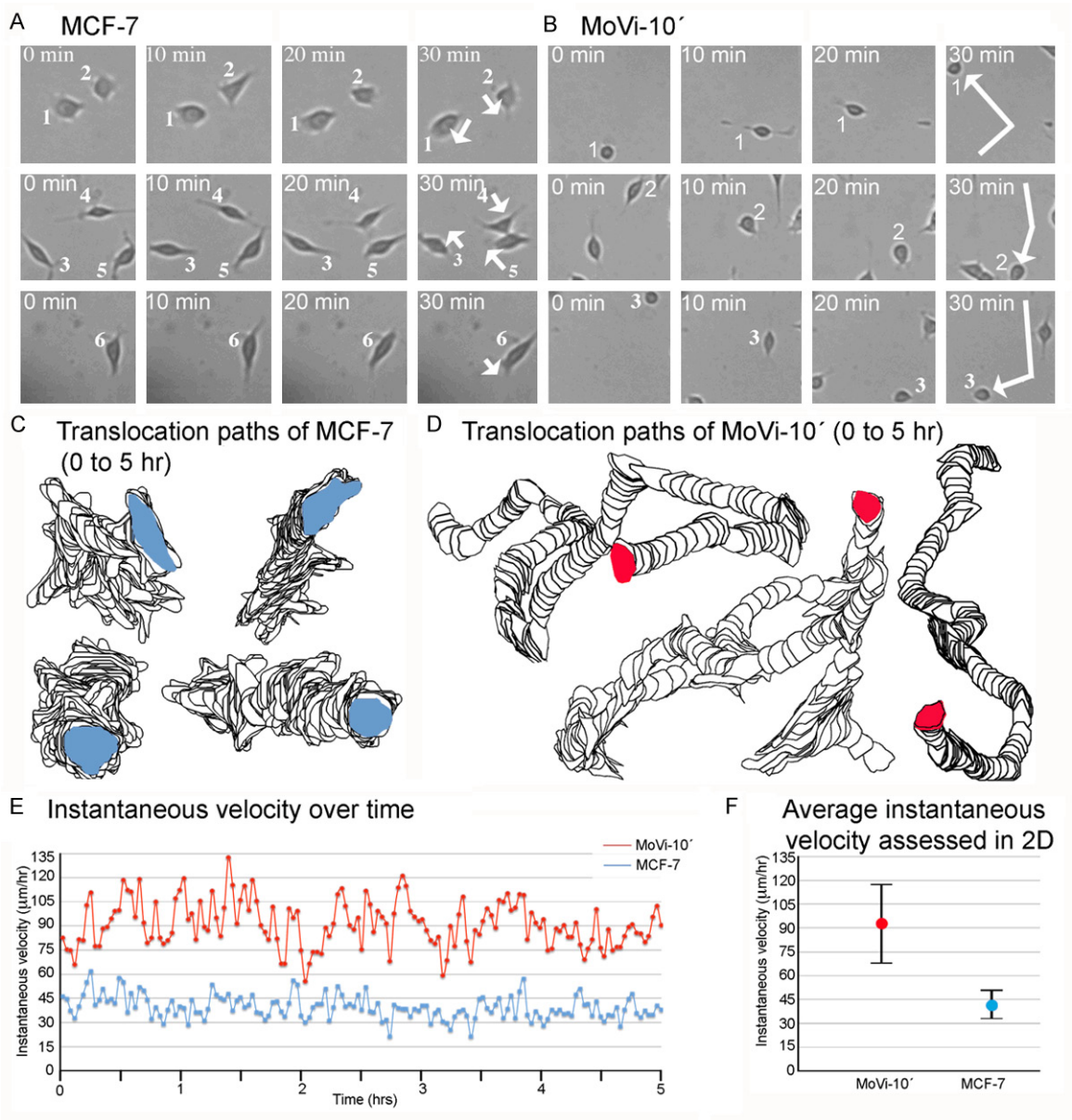

Figure 2. 2D computer-assisted analysis of single cell motility reveals that MoVi-10´ cells are on average twice as fast as MCF-7 cells. Motility was assessed on the surface of a Matrigel film. A. Phase contrast images over a 30 minute period, of representative MCF-7 cells. The arrows in 30 min panels denote extent and net direction of cellular translocation. B. Phase contrast images over a 30 minute period, of representative MoVi-10´ cells. The arrows denote in 30 min panels extent and net direction of cellular translocation. C. Computer-generated perimeter tracks of representative MCF-7 cells over a five hour period. Colored image represents cells at last time point. D. Computer-generated perimeter tracks of representative MoVi-10´ cells over a five hour time period. E. Instantaneous velocity plotted as a function of time averaged for 20 MCF-7 and 25 MoVi-10´ cells. F. Mean instantaneous velocity for the 20 MCF-7 and 15 MoVi-10´ cells analyzed in panel E. Error bar represents standard deviation.

line, through transfection with the vector LK-444 [47] containing the full-length mouse open reading frame of the vimentin cDNA, under the control of the ß-actin promoter [48]. MoVi-10´ cells formed significantly larger tumors when injected into the mouse mammary pad than the parental MCF-7 cells [29]. An analysis of vimentin expression by the reverse transcription-polymerase chain reaction (RT-PCR) confirmed that transcription of vimentin was high in derivative MoVi-10´ cells and undetectable in MCF-7 cells under the same conditions (**Figure 1**). RT-PCR

Table 1. Motility and morphology parameter reveal that individual MoVi-10´ cells are more motile than individual MCF-7 cells

Cell type	N	Total path length (m)	Instantaneous velocity (μm/hr)	Positive flow (%)	Persistence	Area (mm^2)
MCF-7	20	246.2 ± 45.5	44.4 ± 8.1	11.5 ± 2.4	0.26 ± 0.14	458.0 ± 82.3
MoVi-10´	25	507.7 ± 127.4	94.3 ± 23.9	27.1 ± 9.6	0.23 ± 0.18	297.5 ± 66.7
P-values		0.0076	0.00072	0.0210	NS	0.100

Values are presented as means ± standard deviation. NS, not significant.

analysis also revealed that vimentin was expressed at higher levels in the cell lines MDA-MB-435α6HG6 and SUM149 cells, which undergo coalescence [24] and unpublished observations, than in MCF-10A cells, which do not undergo coalescence [24], suggesting a correlation between vimentin expression and coalescence (**Figure 1**). Immunostaining with 40E-C, a monoclonal antibody against vimentin, confirmed that vimentin was over-expressed and correctly localized in MoVi-10´ cells (data not shown). It had previously been shown that MoVi-10´ cells invaded a laminin/collagen-coated Millipore filter in a Boyden chamber at twice the rate of MCF-7 cells [29]. These results were interpreted to mean that individual MoVi-10´ cells were more motile than MCF-7 cells. To test this directly, MCF-7 and MoVi-10´ cells were plated at low density on the surface of a slide coated with Matrigel and single cell behavior was recorded in 2D at 2 minute intervals for 24 hours. Phase contrast images of representative MoVi-10´ and MCF-7 cells are presented at 10 minute intervals over a 30 minute period in **Figure 2A** and **2B**, respectively. The net translocation tracks (compare arrows in **Figure 2A** and **2B**) suggested that MoVi-10´ cells were far more motile than MCF-7, as previously inferred from Boyden chamber experiments [29]. Computer-generated 2D perimeter tracks of cells also suggested that MoVi-10´ cells traveled longer distances in the same time interval (5 hours) than MCF-7 cells on the Matrigel surface (**Figure 2C** and **2D**, respectively), within the same time interval. Computer-assisted measurements of instantaneous velocity over a five hour period of analysis [33, 34] revealed that on average individual MoVi-10´ cells were approximately twice as fast as individual MCF-7 cells (**Figure 2E**). The mean instantaneous velocity (± standard deviation) of 20 MCF-7 and 25 MoVi-10´ cells over the five hour period was 44.4 ± 8.1 and 94.3 ± 23.9 μm per hour (**Figure 2F**). The difference was highly significant (*P* value of 0.00072). The instantaneous velocity of the individual MoVi-10´ cells was also significantly higher than other tumorigenic cell lines derived from breast cancer, such as MDA-MB-435α6HG6, which exhibited an instantaneous velocity of 36.8 ± .09 μm per hour under similar conditions. Measurements of the parameter "positive flow", which is computed as the displacement of cell area per unit time and, hence, is not based on the cell centroid [34], also revealed that the translocation of MoVi-10´ on a surface was more than twice that of MCF-7 (**Table 1**). However, the mean persistence of translocation, measured as the net path divided by the total path [34, 49, 50] was similar for MCF-7 and MoVi-10´ cells (**Table 1**). Quantitative analyses of area suggested that MCF-7 cells were on average either larger or flatter than in MoVi-10´ cells (**Table 1**).

Coalescence in MCF7 and MoVi-10´ mixtures

We previously showed that when cells from tumorigenic cell lines and cells cultured from fresh tumor tissue were seeded in a 3D Matrigel matrix, they multiplied to form individual clonal islands or primary aggregates that then coalesced to form very large aggregates [24]. Eventually, most of the primary aggregates in a territory of Matrigel were incorporated into one massive aggregate that in some cell lines formed, in time, a hollow sphere with a differentiated architecture [24]. In marked contrast, cells from non-tumorigenic or very weakly tumorigenic lines, and fresh non-cancerous tissue seeded in Matrigel, formed clonal aggregates through cell multiplication, but these aggregates did not coalescence [24]. These alternative scenarios were observed in cell preparations from a variety of tumorigenic cell lines and cells from fresh tumor tissues [24].

First using traditional light microscopy, we tested whether these alternative scenarios held for the highly tumorigenic derivative MoVi-10´ and

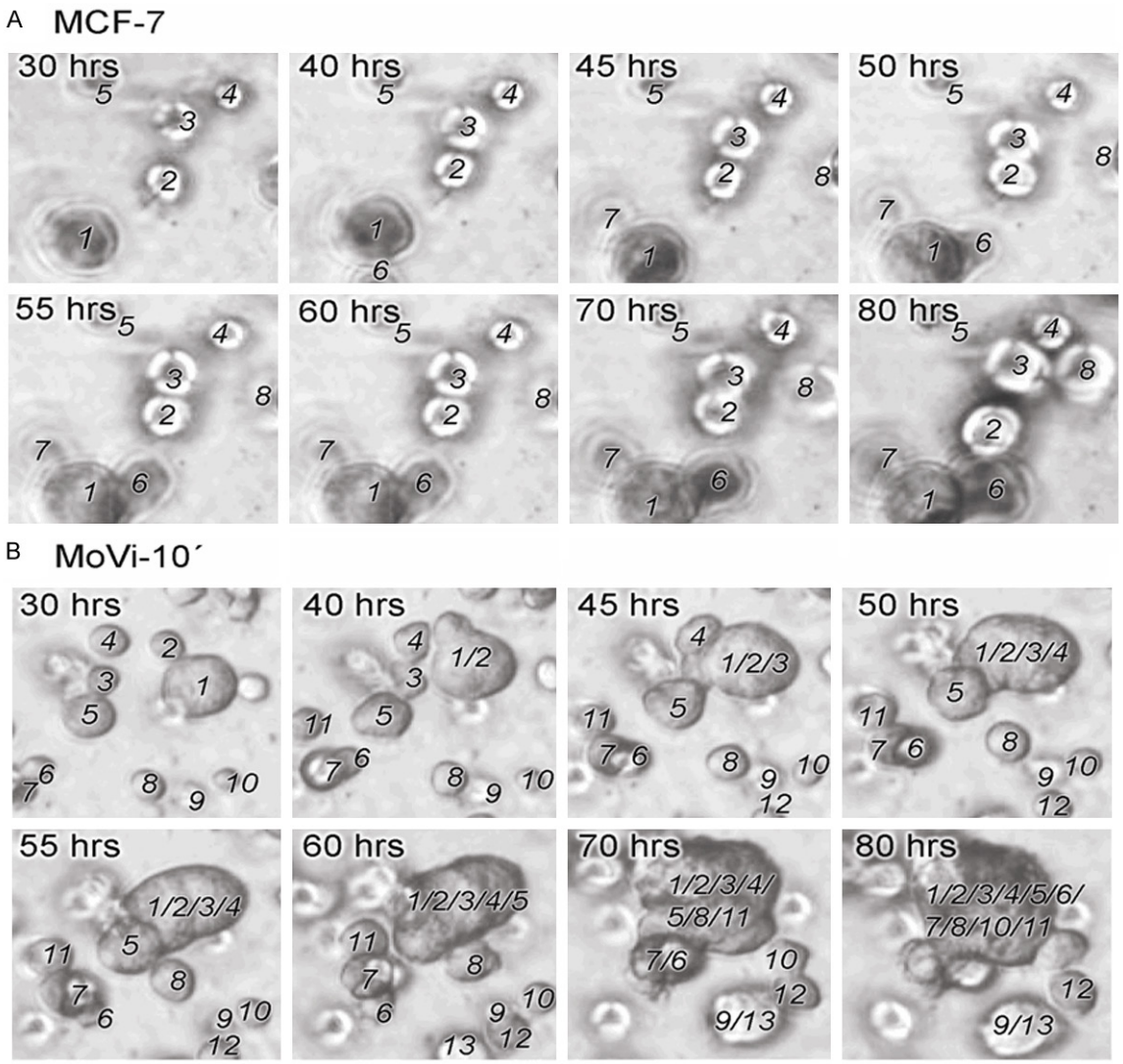

Figure 3. Phase contrast microscopy images over a 50-hour period of aggregates in a 3D Matrigel reveal that MoVi-10´, but not MCF-7, undergo primary aggregate coalescence. A. MCF-7 aggregates. B. MoVi-10´ aggregates. Aggregates are numbered. After a fusion, the coalesced aggregate numbers are combined with slashes between. Micrographs were all taken through phase contrast microscope with a 4X objective at a fixed distance.

the weakly tumorigenic parent cell line MCF-7. Homogeneous populations of each strain were cultured in 3D in Matrigel in 5% CO_2 at 37°C. Cultures were imaged in one plane at 200X magnification using phase optics. In **Figure 3A**, the discernable clonal islands at 30 hours that were formed by MCF-7 cells are numbered 1 through 5. At subsequent time points between 30 and 80 hours, three new aggregates, 6, 7 and 8, moved into the plane of view. Through this period of analysis, no coalescence was observed. The same analysis was performed with MoVi-10´ cells. In contrast to MCF-7 cultures, the aggregates formed by MoVi-10´ cells coalesced throughout the period of analysis. In the first 10 hours, the first coalescence occurred between aggregates 1 and 2, and after 50 hours, aggregates 1, 2, 3, 4, 5, 6, 7, 8, 10 and 11 had formed a single, large aggregate, 1/2/3/4/5/6/7/8/10/11 (**Figure 3B**). A previously reported [24], the largest aggregate, in this case aggregate 1, acted as the focal point for coalescence with smaller aggregates.

3D reconstruction of coalescence

We next generated high-resolution 3D reconstructions over time (4D) of MCF-7 and MoVi-10´ preparations embedded in 3D Matrigel (**Figure 4**) using the "complexity-based bitmap

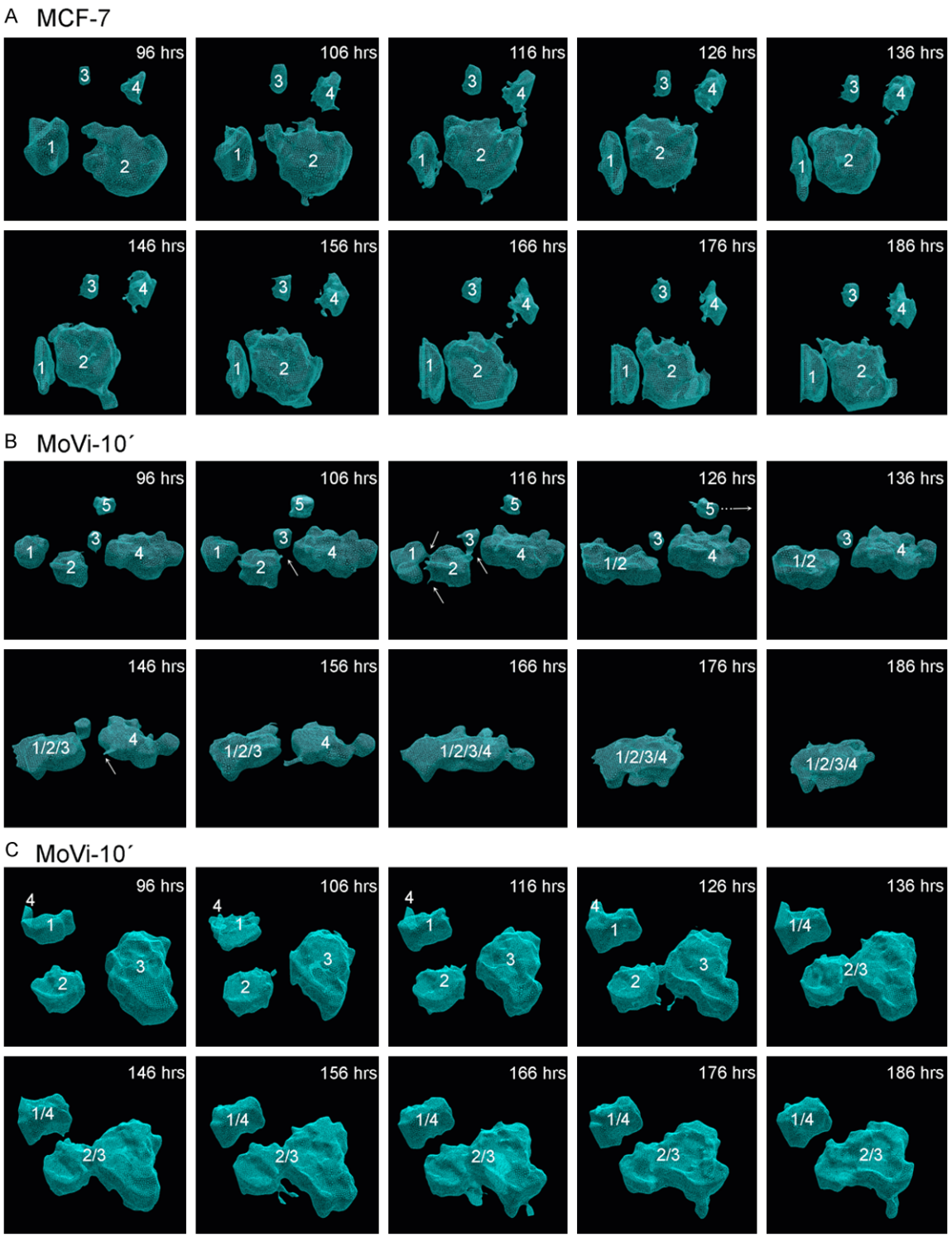

Figure 4. J3D-DIAS 4.1 reconstructions of a region of aggregates in Matrigel over a 90 hour period beginning at 96 hours and ending at 186 hours reveal that primary aggregates of MoVi-10´, but not MCF-7, undergo coalescence. A. A representative field of four MCF-7 primary aggregates. Note that there is no coalescence. B, C. Two different fields of four MoVi-10´ aggregates. Note coalescence in each case.

object detection" software C-BBOD in the J3D-DIAS 4.1 software program [23-25]. A 4D real time measurement of living cells embedded in matrix allows identification of behaviors that

either do not occur on a 2D substrate [51] or are not resolvable with standard light microscopy [52]. Each reconstruction of aggregates presented in **Figure 4** included three in a 3D viewing region of interest and was based on 150 optical sections, at 10 μm increments, through 1500 μm in the Z-axis [24]. 3D reconstructions obtained over the 90 hour period, between 96 and 186 hours are presented in **Figure 4A** for MCF-7 preparations and **Figure 4B** and **4C** for two MoVi-10´ preparations. In the MCF-7 field of analysis, there were four aggregates at 96 hours. Subsequently, the aggregates underwent changes in shape, which included some protrusion of cells from the aggregate surfaces, for instance at the bottom of aggregate 2 at 146 hours (**Figure 4A**). However, even when MCF-7 aggregates came in contact, as in the case of aggregates 1 and 2, at 176 hours, they did not coalesce (**Figure 4A**).

In marked contrast, 3D reconstructions of MoVi-10´ preparations revealed a high degree of coalescence over the same time period (**Figure 4B**, **4C**). In the region of analysis in **Figure 4B**, there were five initial aggregates at 96 hours. By 116 hours, cells had extended from aggregates 2 and 3 towards each other and established contact (arrows). At the same time, several protrusions emerged from aggregate 2 in the direction of aggregate 1, resulting in coalescence to form aggregate 1/2 by 126 hours. Aggregate 1/2 then coalesced with aggregate 3 146 hours (**Figure 4B**). At 146 hours, aggregate 4 extended a protrusion towards aggregate 1/2/3, generating through coalescence aggregate 1/2/3/4 at 166 hours (**Figure 4B**). Thus all of the initial aggregates at 96 hours had coalesced by 166 hours (**Figure 4B**). The composite aggregate compacted between 166 and 186 hours. Aggregate 5 exited the field of view between 126 and 186 hours (**Figure 4B**). In a repeat experiment presented in **Figure 4C**, four aggregates at 96 hours coalesce into 1/4 and 2/3 between 96 and 186 hours, and these two composites subsequently combined to form aggregate 1/2/3/4 after 200 hours (data not shown).

Quantitative differences in aggregate behavior

Because the original 3D-DIAS software program [33-37, 42, 52] and the upgraded J3D-DIAS 4.1 software program [23-25] convert the final reconstructions into mathematical models, a number of parameters that quantify aggregate behavior can be computed. In the experiment in **Figure 5**, relative aggregate number (i.e., the number normalized to that at 100 hours) in a field of 10 MCF-7 aggregates remained at 100% between 100 and 160 hours, and then dropped to 80% at 170 hours (**Figure 5A**). In contrast, relative aggregate numbers for a field of 12 MoVi-10´ aggregates fell to 10% after 170 hours (**Figure 5A**). Coalescence was also assessed by the "field density" parameter. To compute this parameter, the smallest 3D box that encompasses all the aggregates in a field is constructed at each time point, the volume of aggregates within that bounding box is determined and divided by the box volume. For comparison, the initial ratios, in this case at 80 minutes, were normalized to one. The field density of MCF-7 cells increased by about 33% (**Figure 5B**), due mainly to aggregate growth, while that of MoVi-10´ increased 133% from 1.0 to approximately 2.33 (**Figure 5B**). The large increase in field density of the MoVi-10´ preparation was due to the directed movement of aggregates towards a single focal point and coalescence. The movement of aggregates was assessed by computing the mean instantaneous velocity [34], based on the translocation of the 3D centroid of reconstructed aggregates in the field of analysis over a 90 minute period (**Figure 5C**). The mean velocity of MCF-7 aggregates remained constant at approximately 3 μm per hour, while that of MoVi-10´ aggregates remained at approximately 7 μm per hour, with transient peaks resulting from coalescence events (**Figure 5C**).

Finally, the complexity of aggregates, an indirect reflection of the degree of compactness and cellular movement within an aggregate and at its periphery [23-25], was assessed over time (**Figure 5D**). The mean surface complexity of MCF-7 was relatively stable fluctuating between 1.0 and 1.15. That of MoVi-10´ aggregates remained at approximately 1.3 between 80 and 120 hours, increased to approximately1.4 to 1.5 between 120 and 150 hours, then decreased to approximately 1.2 thereafter (**Figure 5D**). The increase in surface complexity of MoVi-10´ aggregates (**Figure 5D**) correlated with an increase in the rate of coalescence,

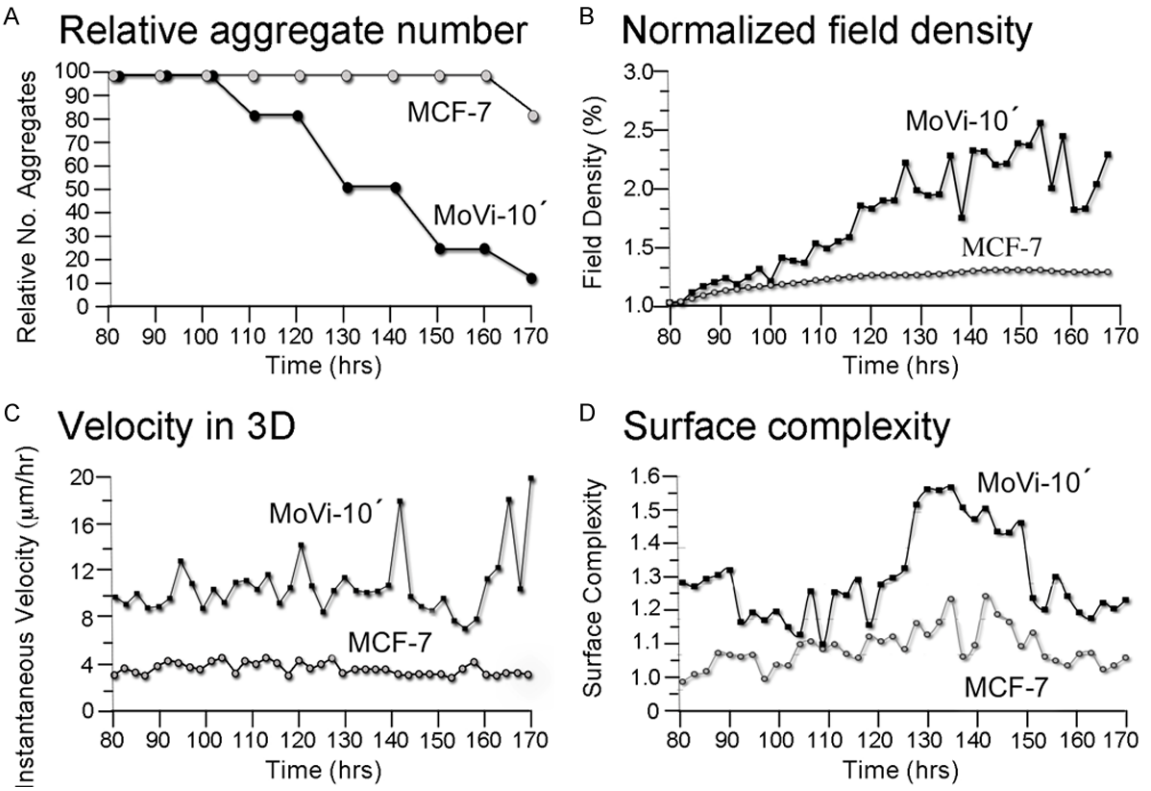

Figure 5. Quantitation of 3D parameters using J3D-DIAS 4.1 reveals that MoVi-10´ primary aggregates coalesce, move faster in the Matrigel matrix, and exhibit more surface complexity than MCF-7 primary aggregates. For each cell line, ten primary aggregates in a single 3D field of analysis were reconstructed in 3D over a 90 hour period using J3D-DIAS 4.1 software, and the resulting mathematical models used to computer parameters. A. The relative number of aggregates, computed as percent of 80 hour reconstruction. B. Field density normalized to that of the 80 hour reconstruction. C. Average instantaneous velocity. D. Average surface complexity.

and the decrease after 15 hours to compaction of the aggregates formed by coalescence (**Figure 5A**, **5B**).

MoVi-10´ aggregates coalesce by forming cellular cables

We previously demonstrated [24] that coalescence between aggregates of the tumorigenic cell line MB-435-Br1 is actively facilitated either by interactions between specialized large, multinucleated facilitator cells released from aggregates and probes extending from the surfaces of aggregate, or by probes alone. In both cases the cells formed cables between aggregates, then the multicellular cables contracted to facilitate coalescence. Analysis of DIC images taken at one depth over time revealed that there was very little cellular activity at the surfaces of neighboring MCF-7 aggregates in the inter-aggregate space (**Figure 6A**). However, cells penetrated the inter-aggregate spaces between MoVi-10´ aggregates during the process of coalescence (**Figure 6B**). To examine the mechanism that mediates coalescence of MoVi-10´ aggregates in 3D, we selected a time series in which the space between two aggregates undergoing coalescence was visible. We used the C-BBOD tracing method for aggregates and the manual tracing option of J3D-DIAS 4.1 software for single cells [23-25]. Single cell reconstructions were then combined with caged aggregate reconstructions. A representative coalescence event, occurring at approximately 24 hours, is presented in **Figure 7**. Three cells, color-coded green, purple and red, can be seen at 120 hours of culture, at the periphery of aggregate 1 penetrating the inter-aggregate space (**Figure 7**). Between 120 and 126 hours, these cells formed an aligned cable that penetrated the space, extending in the direction of aggregate 2 (**Figure 7**). The end of the cable contacted aggregate 2 at 126 hours, forming a bridge (**Figure 7**). Between 129 and

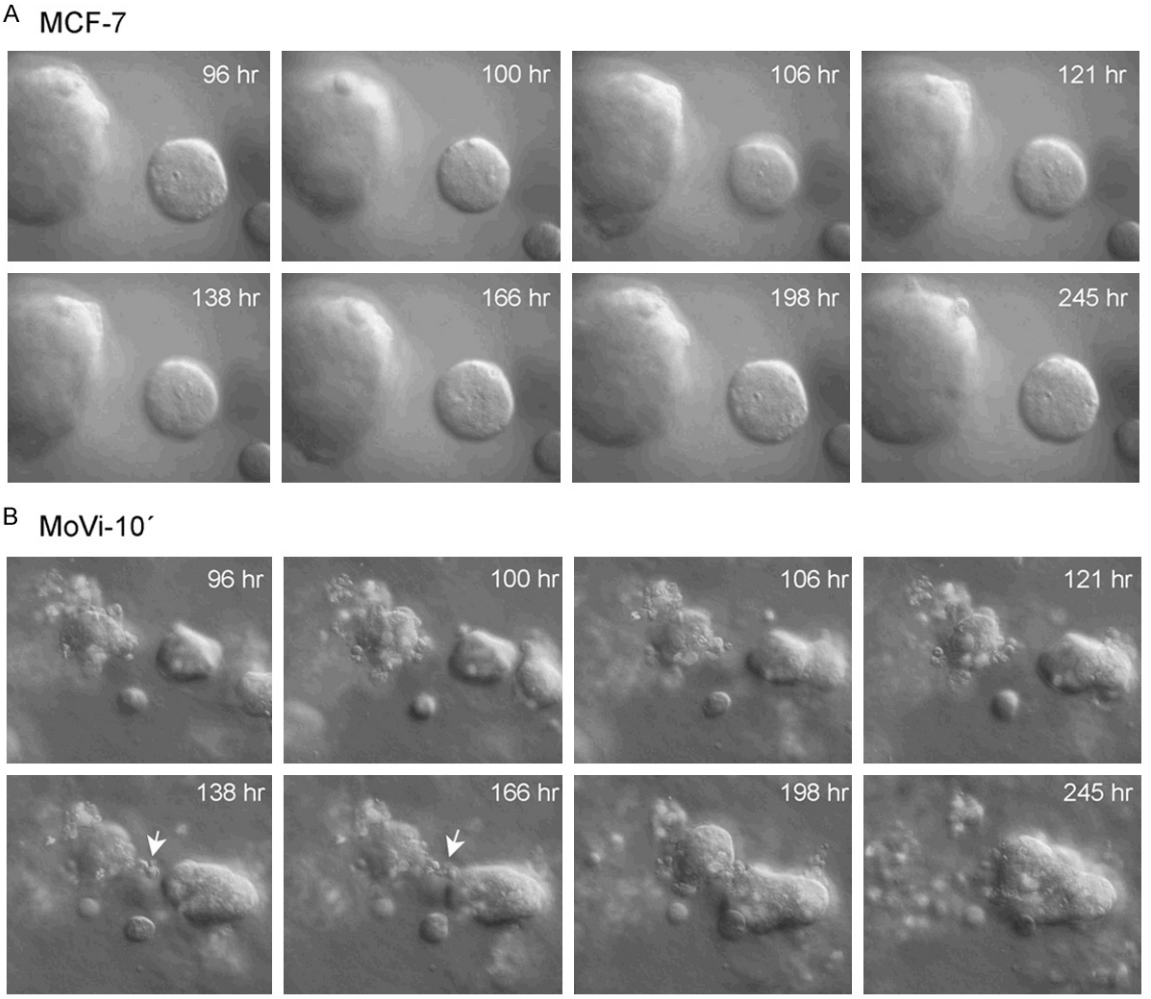

Figure 6. Inter-aggregate regions of MCF-7 preparations are devoid of cells whereas inter-aggregate regions of MoVi-10´ preparations are filled with probing cells. A. DIC images of MCF-7 preparation between 96 and 245 hours. B. MoVi-10´ preparation between 96 and 245 hours. Note coalescence at 198 and 245 hours in the MoVi-10´ preparation. Arrows in panels of 138 and 166 hours of MoVi-10´ preparation point to probing cells in the inter-aggregate space.

144 hours, the bridge contracted and reorganized, bringing the two aggregates together. By 144 hours, the two aggregates no longer had a distinct boundary. In this example aggregate 1 was drawn to aggregate 2. This behavior was observed multiple times between pairs of MoVi-10´ aggregates undergoing coalescence but was never observed in preparations of MCF-7 or non-cancerous cell lines. In Supplementary Movies 1 and 2, the behaviors described for MCF-7 and MoVi-10´ aggregates are presented. These movies represent the DIC images at a single plane in Matrigel preparations followed from 100 to 170 hours. In the MoVi-10´ movie the behavior of the cells forming the cable and coalescence can be discerned.

Minority MoVi-10´ cells induce majority MCF-7 cells to aggregate in two dimensions

Because MoVi-10´ aggregates rapidly coalesce, but MCF-7 aggregates did not, we tested whether minority MoVi-10´ cells could facilitate coalescence in majority MCF-7 cultures. In the first test, mixtures of cells were distributed on a cushion of Matrigel at relatively high density and photographed at 0 and 72 hours. Mixtures included 5%, 10%, 25% and 50% MoVi-10´ cells. Preparations of 100% MCF-7 and 100% MoVi-10´ cells were also tested. Qualitatively, the number of individual cells and aggregates at 72 hours, when compared to the original number of cells in the Matrigel surface at 0

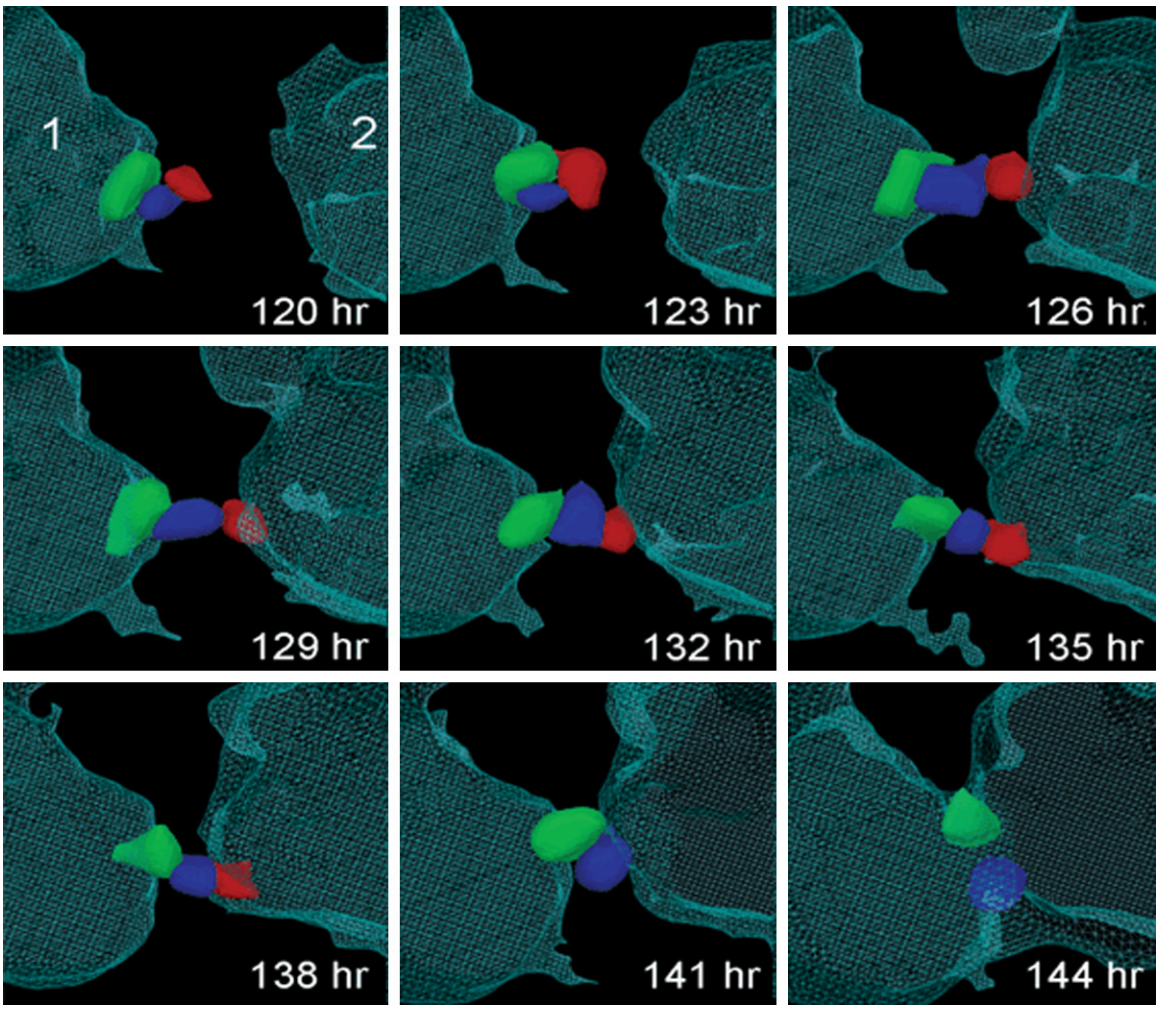

Figure 7. Coalescence is achieved in MoVi-10´ cultures through the formation of cellular bridges that then contract, moving the smaller aggregate, in this case aggregate 1, into the larger one, aggregate 2. Aggregates were reconstructed by J3D-DIAS 4.1 using C-BBOD for automatically tracing and reconstructing aggregates and manual tracing for cells. Single cells forming the bridge are color-coded solid green, purple and red.

hours, was less in the mixtures of MCF-7 and MoVi-10´ cells, and the 100% MoVi-10´ cultures than it was in the 100% MCF-7 culture (**Figure 8A**). We then plotted the percent decrease in the number of individual cells plus aggregates between 0 and 72 hours, as a function of time (**Figure 8B**). For 100% MCF-7 cells, there was a 27 ± 6% decrease, but for 5% and 10% mixture, there was a 75 ± 5 and 79 ± 4% decrease (**Figure 8B**). Interestingly, as more MoVi-10´ cells were added (25 and 50%), the percent gradually became less. For 100% MoVi-10´ cell preparations, the decrease in the number of cells plus aggregates at 72 hours was 55%. These results suggested that MoVi-10´ facilitated MCF-7 coalescence.

Minority MoVi-10´ cells induce minority MCF-7 aggregates to coalesce in 3D

We next tested whether minority MoVi-10´ cells induced majority MCF-7 cells to coalesce in a 3D Matrigel model. In **Figure 9**, a single area of aggregates formed by a mixture of 10% MoVi-10´ cells and 90% MCF-7 cells in the 3D Matrigel model is reconstructed from 55 hours to 105 hours using the C-BBOD automatic object identification feature in J3D-DIAS 4.1. In the selected field of analysis there were 10 aggregates (**Figure 9A**). To verify the independence of the 10 aggregates at 50 hours, we rotated the field to observe all surfaces (Supplementary Figure 1). During rotation, the

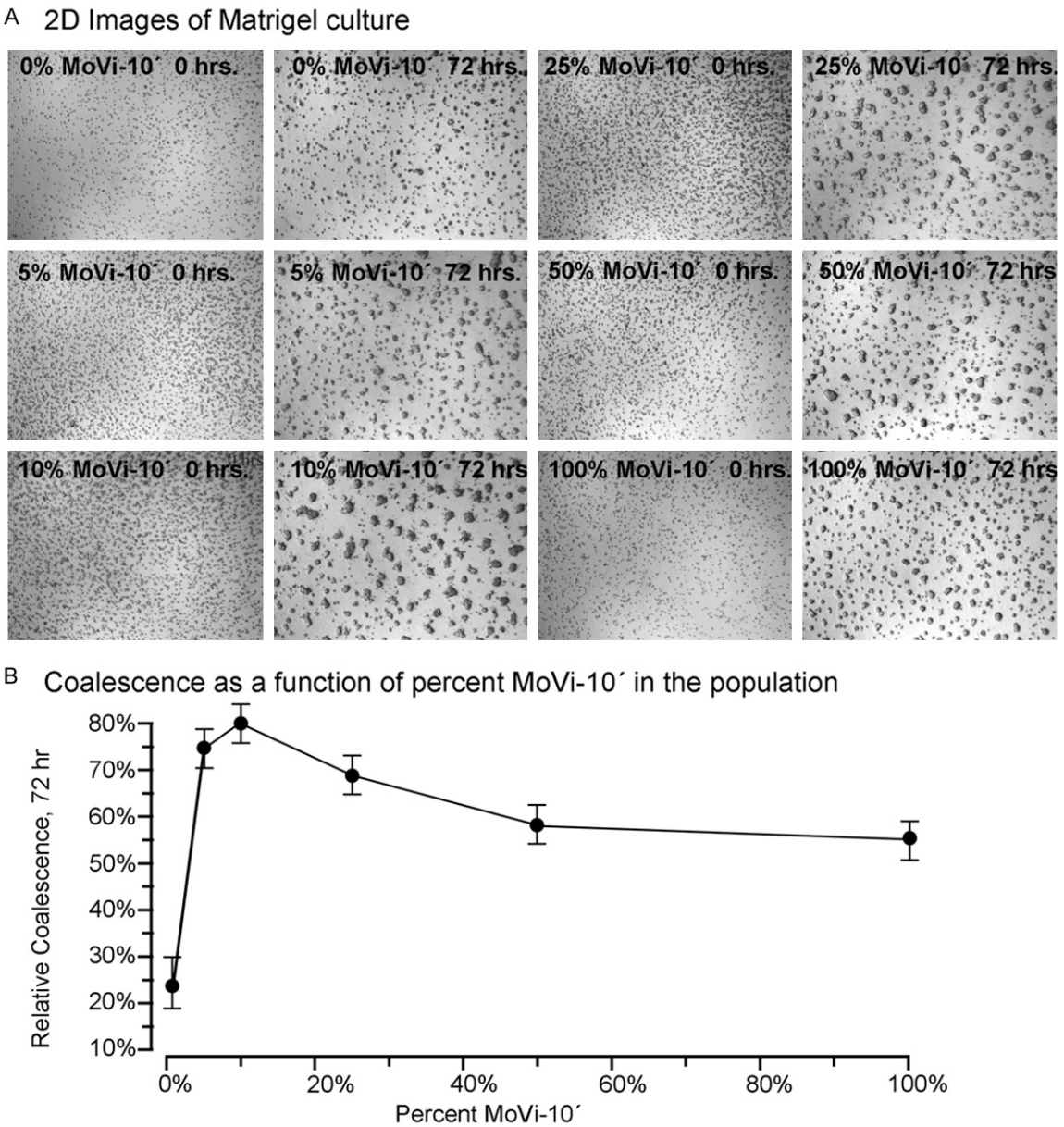

Figure 8. A minority of MoVi-10´ cells will induce coalescence by majority MCF-7 cells on a 2D Matrigel surface. Coalescence was assessed by distributing cells on a Matrigel surface, then overlaying the 2D model with a second coat of Matrigel. A. Phase contrast micrographs are presented of cell preparations at 0 and 72 hours for 0% MoVi-10´; 100% MCF-7; 5% MoVi-10´, 95% MCF-7; 10% MoVi-10´, 90% MCF-7; 25% MoVi-10´, 75% MCF-7; 50% MoVi-10´, 50% MCF-7; and 100% MoVi-10´, 0% MCF-7 cells. B. The percent coalescence at 72 hours as function of percent MoVi-10´ cells.

aggregates in the front of the reconstruction appear larger, and when rotated to the back of the field, appear smaller. All aggregates at 50 hours proved to be independent (Supplementary Figure 1). Through the 55 hours of analysis, aggregates 1, 2, 3, 4, 7 and 8 coalesced to form aggregate 1/2/3/4/7/8, and aggregates 5 and 6, and 9 and 10, coalesced to form aggregates 5/6 and 9/10 (**Figure 9**). This result was obtained in repeat experiments. As demonstrated in **Figures 3A** and **4A**, a 100% MCF-7 aggregates formed by the multiplication of cells seeded in the 3D Matrigel model did not coalescence. These results verify that a minority of MoVi-10´ cells induce coalescence of MCF-7 aggregates.

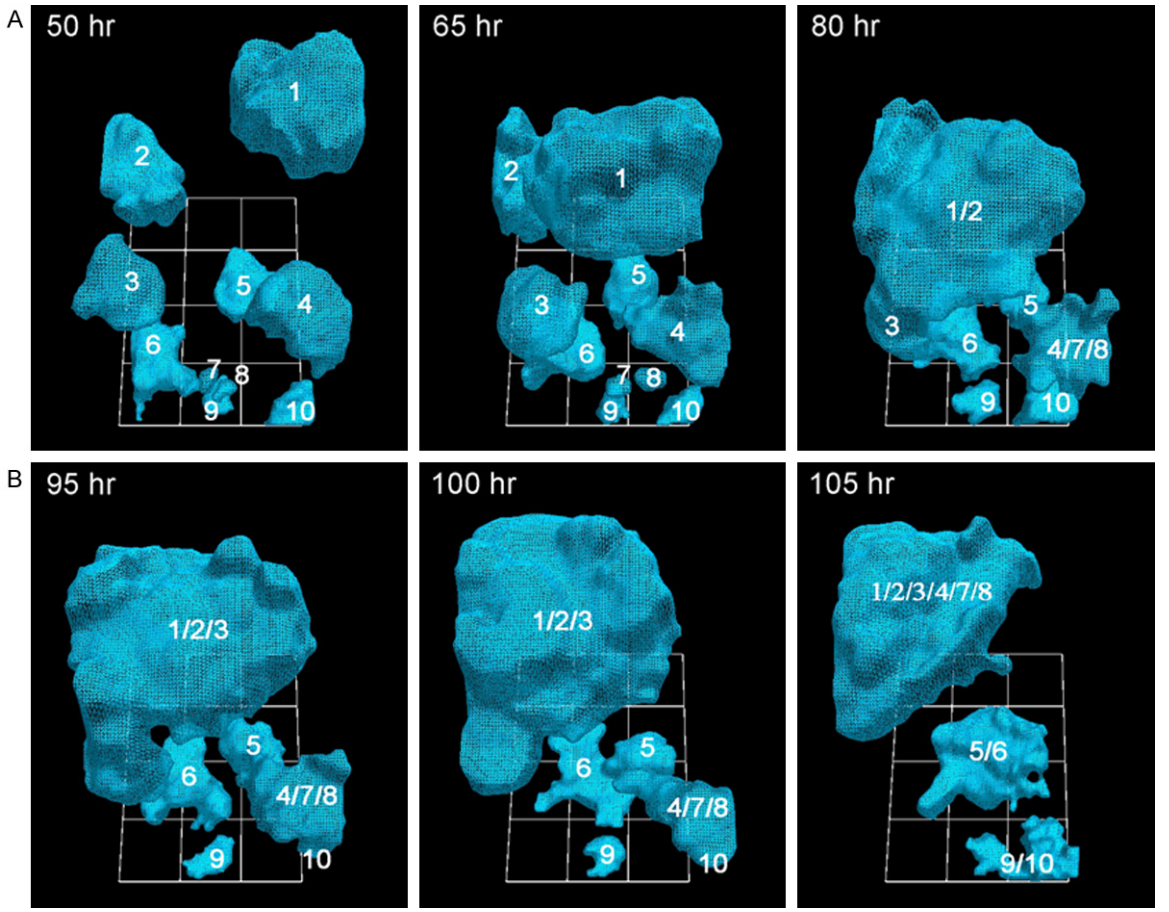

Figure 9. Using J3D-DIAS 4.1 software, 3D reconstructions over a 55 hour period revealed that primary aggregates of a mixture of 10% MoVi-10´ cells and 90% MCF-7 cells undergo coalescence. Coalescence occurred between primary aggregates 1, 2, 3, 4, 7 and 8, aggregates 5 and 6, and aggregates 9 and 10. Rotation of the 50 hour preparation in Supplementary Figure 1 shows all primary aggregates are initially independent.

MCF-7 coalescence is facilitated by the formation of MoVi-10´ cables

Since the coalescence of MoVi-10´ aggregates is facilitated by the formation and contraction of cellular cables, we tested the possibility that minority MoVi-10´ facilitated the coalescence of MCF-7 aggregates by forming MoVi-10´ cables. To accomplish this, MCF-7 cells expressing green fluorescent protein, were mixed with unlabeled MoVi-10´ cells in the 3D Matrigel model at a 9:1 ratio, and incubated for 48 hours. Aggregates and intervening spaces were then visualized simultaneously by DIC and fluorescence microscopy. The fluorescent images, DIC images and colored cellular bridges are presented in **Figure 10** for four sets of aggregates and their intervening spaces. In each case, the cells in the aggregates were composed primarily of fluorescent MCF-7 cells, whereas the cells forming cables in the intervening spaces contained no MCF-7 cells (**Figure 10A-D**). In the interspaces between aggregates in **Figure 10A** and **10B**, examples are presented of cellular bridges between two aggregates. In both cases, the bridges are composed exclusively of unlabeled MoVi-10´ cells. In **Figure 10C** and **10D**, examples are presented of MoVi-10´ cells in an intervening space extending pseudopods and filopodia to multiple MCF-7 aggregates. Ten interspace regions were imaged and found to contain non-fluorescent MoVi-10´ cells in the cables and inter-aggregate spaces. Such connections and bridges were not formed in inter-aggregate spaces of preparations formed by homogeneous populations of MCF-7 cells of the cell line expressing GFP. These results demonstrate that minority MoVi-10´ cells facilitate coalescence between aggregates of MCF-7 cells by forming cables that then bring together MCF-7 aggregates.

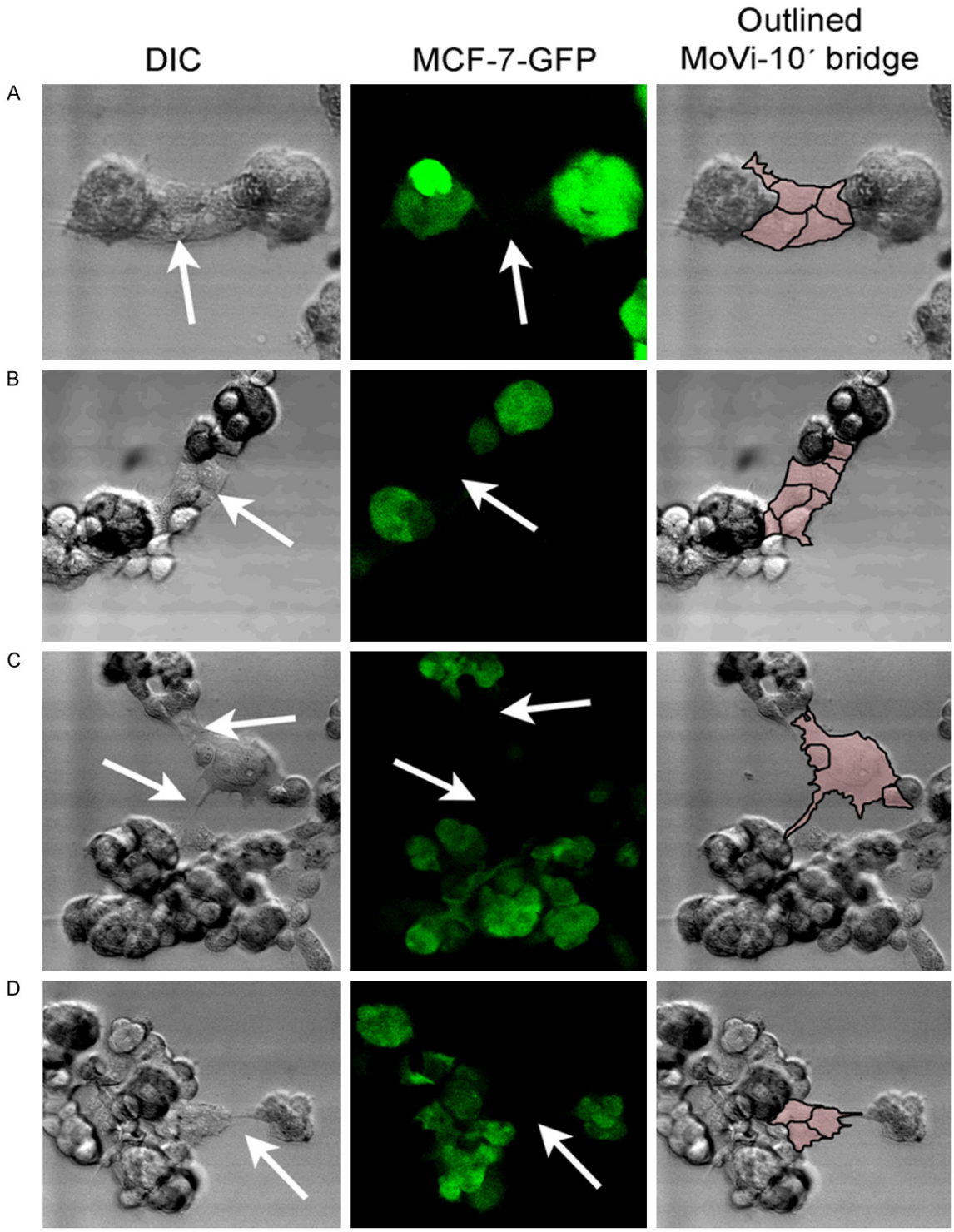

Figure 10. Minority MoVi-10´ cells facilitate coalescence of majority MCF-7 cell primary aggregates by forming cellular bridges. 90% MCF-7 cells expressing green fluorescent protein were mixed with 10% unlabeled MoVi-10´ cells and seeded in 3D Matrigel. Primary aggregates attached by cellular bridges were first imaged with DIC optics to view all cells, then with fluorescence microscopy to view only MCF-7 cells. Note that the bridges between primary aggregates (white arrows) were composed only of unlabeled MoVi-10´ cells. A-D. Representative examples in which the cellular bridges are formed exclusively by nonfluorescent MoVi-10´ cells. For each of the four examples, we have outlined and colored in pink the unlabeled MoVi-10´ cells forming the bridges, in the last of the three panels.

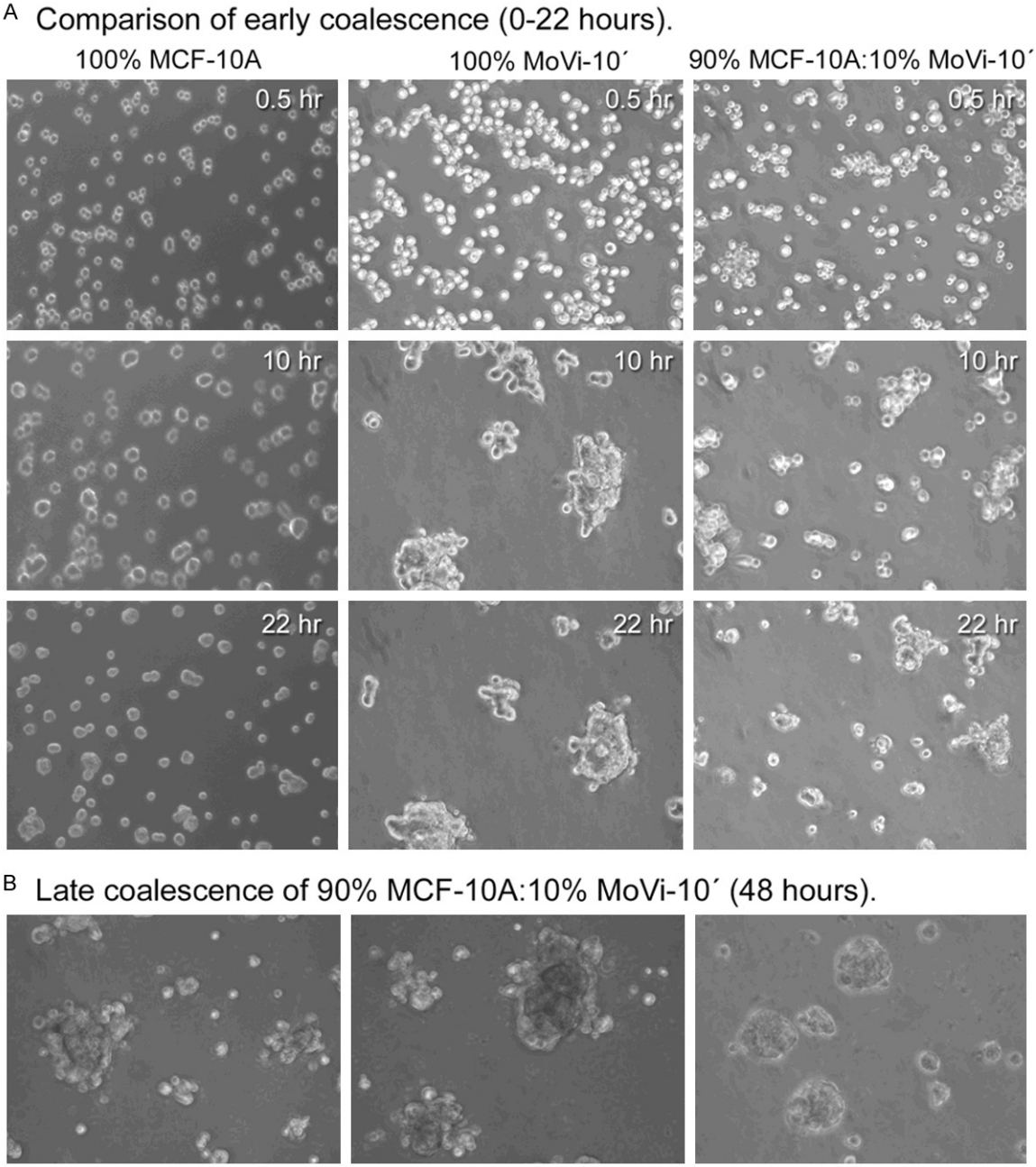

Figure 11. MoVi-10´ mediates coalescence in preparations of the non-tumorigenic cell line MCF10A. Cells were dispersed on a Matrigel film, which was then overlaid with a layer of Matrigel. Preparations were examined in 2D at 10× magnification using phase optics. A. The mediation of coalescence by 22 hours. Preparation included 100% MCF-10A; 100% MoVi-10´; and 90% MCF-10A, 10% MoVi-10´ cells. For each preparation, images are shown at 0.5, 10 and 22 hours. Note that 10% MoVi-10´ cells, 90% MCF-10 cells undergo coalescence by 22 hours, but not to the extent of 100% MoVi-10´ preparations. B. At 48 hours, coalescence of the 90% MCF10A, 10% MoVi-10´ preparations is close to that of the 100% MoVi-10´ preparations.

MoVi-10´ mediates coalescence of a non-cancerous epithelial cell line

Since the tumorigenic, coalescing cell line MoVi-10´ was derived from weakly tumorigenic, non-coalescing MCF-7 cell line, the facilitation of coalescence may reflect a compatibility and exclusiveness related to pedigree. We therefore tested whether MoVi-10´ also facilitated coalescence of the non-cancerous breast epithelial cell line MCF-10A, which is unrelated [28]. This line, like MCF-7, does not undergo

aggregate coalescence in the 3D Matrigel model [24]. Mixing experiments of MoVi-10´ and MCF-10A in a ratio of 1:9 resulted in the induction of coalescence of majority cell aggregates through 22 hours (**Figure 11A**). Although the extent of coalescence at 22 hours was not as pronounced as in pure MoVi-10´ cultures, by 48 hours, aggregates in the 90% MCF-10A: 10% MoVi-10´ cultures were comparable to the 22 hour aggregates on 100% MoVi-10´ cultures (**Figure 11B**).

Discussion

Using the 3D Matrigel model and the computer-assisted reconstruction and motion analysis system J3D-DIAS-4.1 [23-25], we previously discovered several new characteristics of tumorigenic cell lines not shared with non-tumorigenic or weakly tumorigenic cell lines [24]. First we found that when tumorigenic cell lines or cells cultured from fresh tumors were seeded in a 3D Matrigel, they formed primary aggregates by cell multiplication, which then coalesced to form larger aggregates that in time differentiated into spherules. The coalescence of aggregates was accomplished through two related scenarios. In the first, large, multinucleated facilitator cells exited the aggregate and interacted with cells at the aggregate surface, which extended filopodia but did not exit the aggregate ("probes"). The two cell types formed cellular cables that contracted, drawing smaller aggregates into larger ones. In the second scenario, "probes" at the aggregate surfaces extended into the inter-aggregate spaces without leaving the aggregates. Once contact between probes from the two separate aggregates was established, additional cells crawled out of the aggregates and became entwined around the original cell extensions, forming a cellular cable. These cables contracted, pulling the smaller to the larger aggregate. The aggregate then coalesced. When non-tumorigenic cells were seeded in the same 3D Matrigel model, they multiplied to form primary aggregates, but the formation of specialized facilitator and probe cells was absent, and coalescence did not occur. The cell lines that underwent coalescence included MDA-MB-435-BR1, MDA-MB-435-α6HG6, MoVi-10´, LN18, U87, MARI 011, MARI 023, MARI-028, MARI M2 [24] and MDA-MB-231. The cell lines that did not undergo coalescence included MCF-10A, MARI 027 and MCF-7 [24].

Here, we have tested whether minority cells from a highly tumorigenic and motile cell line, MoVi-10´, which rapidly undergoes aggregate coalescence in 3D Matrigel, could induce majority cells of the weakly tumorigenic parental cell line, MCF-7, derived from the pleural effusion of a metastatic breast cancer patient [53], to undergo coalescence. We found that as little as 5% MoVi-10´ cells facilitated coalescence of aggregates composed primarily of MCF-7 cells, which by themselves did not undergo primary aggregate coalescence. We also found the minority MoVi-10´ cells mediated coalescence between primary aggregates of a completely unrelated, non-cancerous epithelial cell line, MCF-10A [28], which had previously been shown to be incapable of undergoing coalescence [24].

Increased motility of MoVi-10´ cells

The tumorigenic MoVi-10´ cell line, which overexpresses the intermediate filament vimentin, was derived from the breast cancer cell line MCF-7 [29]. Hendrix et al. [29] demonstrated that MoVi-10´ cells were more invasive than their parent cell line, MCF-7, penetrating a filter in a Boyden chamber at twice the rate. Here, we extend those findings using computer-assisted single cell analysis [33, 34] to show that MoVi-10´ cells are twice as fast as MCF-7 cells on a 2D Matrigel surface. This increase in single cell motility correlates with the high level of coalescence and cell activity within MoVi-10´ aggregates. It should be noted that as is the case for increased motility [54-56], we show here that the capacity to undergo coalescence correlates with an increase in the expression of vimentin. However, our goal here was not to study the role of vimentin, but to exploit the vimentin overexpressor, MoVi-10´, which undergoes coalescence very rapidly and aggressively, to test our hypothesis.

MoVi-10´ and the formation of cellular cables

The mechanism by which minority MoVi-10´ cells facilitate coalescence is quite remarkable. After individual cells seeded in Matrigel multiply and form clonal islands, or primary aggregates, cells actively enter inter-aggregate spaces and form cables that bring together the aggregates in the process of coalescence. The behavior of MoVi-10´ cells in these cables is reminiscent of the behavior of myofibroblasts in

wound healing [57], and the behavior of secondary mesenchymal cells in sea urchin development [58]. Indeed, MoVi-10´ was generated [29] because of the role vimentin appears to play in the epithelial to mesenchymal transition [59] and the increase in motility caused by vimentin expression in metastatic cells [54, 56, 60]. Here, we have demonstrated that a minority of MoVi-10´ will mediate coalescence between primary aggregates of weakly tumorigenic or non-tumorigenic cells, which alone do not undergo coalescence, by actively forming cables between them. Only the MoVi-10´ cells form the cables, indicating that they do not induce that capacity in non-coalescing cells.

Implications

The results presented here extend our original observation that tumorigenic cell lines and fresh tumor cells possess the unique capacity to undergo coalescence through the active formation of cellular cables [24]. More importantly, they also provide a possible mechanism for how multiple foci may be brought together in a cancerized epithelial field, and a possible explanation, at least in part, for how non-tumorigenic cells, including fibroblasts and endothelial cells [61], can be actively pulled into a growing tumor and comprise the majority of the cells in a tumor.

Disclosure of conflict of interest

None.

Address correspondence to: David R Soll, Developmental Studies Hybridoma Bank, Department of Biology, The University of Iowa, Iowa City, IA 522-42, USA. Tel: 319-335-1117; Fax: 319-335-2772; E-mail: david-soll@uiowa.edu

References

[1] Al-Hajj M, Wicha MS, Benito-Hernandez A, Morrison SJ and Clarke MF. Prospective identification of tumorigenic breast cancer cells. Proc Natl Acad Sci U S A 2003; 100: 3983-3988.

[2] Li C, Heidt DG, Dalerba P, Burant CF, Zhang L, Adsay V, Wicha M, Clarke MF and Simeone DM. Identification of pancreatic cancer stem cells. Cancer Res 2007; 67: 1030-1037.

[3] O'Brien CA, Pollett A, Gallinger S and Dick JE. A human colon cancer cell capable of initiating tumour growth in immunodeficient mice. Nature 2007; 445: 106-110.

[4] Singh SK, Hawkins C, Clarke ID, Squire JA, Bayani J, Hide T, Henkelman RM, Cusimano MD and Dirks PB. Identification of human brain tumour initiating cells. Nature 2004; 432: 396-401.

[5] Blagden SP. Harnessing Pandemonium: The Clinical Implications of Tumor Heterogeneity in Ovarian Cancer. Front Oncol 2015; 5: 149.

[6] De Sousa E Melo F, Vermeulen L, Fessler E, Medema JP. Cancer heterogeneity–a multifaceted view. EMBO Rep 2013; 14: 686-695.

[7] Greaves M and Maley CC. Clonal evolution in cancer. Nature 2012; 481: 306-313.

[8] Gerlinger M, Horswell S, Larkin J, Rowan AJ, Salm MP, Varela I, Fisher R, McGranahan N, Matthews N, Santos CR, Martinez P, Phillimore B, Begum S, Rabinowitz A, Spencer-Dene B, Gulati S, Bates PA, Stamp G, Pickering L, Gore M, Nicol DL, Hazell S, Futreal PA, Stewart A and Swanton C. Genomic architecture and evolution of clear cell renal cell carcinomas defined by multiregion sequencing. Nat Genet 2014; 46: 225-233.

[9] Marusyk A, Almendro V and Polyak K. Intra-tumour heterogeneity: a looking glass for cancer? Nat Rev Cancer 2012; 12: 323-334.

[10] Medema JP. Cancer stem cells: the challenges ahead. Nat Cell Biol 2013; 15: 338-344.

[11] Valent P, Bonnet D, De Maria R, Lapidot T, Copland M, Melo JV, Chomienne C, Ishikawa F, Schuringa JJ, Stassi G, Huntly B, Herrmann H, Soulier J, Roesch A, Schuurhuis GJ, Wohrer S, Arock M, Zuber J, Cerny-Reiterer S, Johnsen HE, Andreeff M and Eaves C. Cancer stem cell definitions and terminology: the devil is in the details. Nat Rev Cancer 2012; 12: 767-775.

[12] Lochhead P, Chan AT, Nishihara R, Fuchs CS, Beck AH, Giovannucci E and Ogino S. Etiologic field effect: reappraisal of the field effect concept in cancer predisposition and progression. Mod Pathol 2015; 28: 14-29.

[13] Slaughter DP, Southwick HW and Smejkal W. Field cancerization in oral stratified squamous epithelium; clinical implications of multicentric origin. Cancer 1953; 6: 963-968.

[14] Chu TY, Shen CY, Lee HS and Liu HS. Monoclonality and surface lesion-specific microsatellite alterations in premalignant and malignant neoplasia of uterine cervix: a local field effect of genomic instability and clonal evolution. Genes Chromosomes Cancer 1999; 24: 127-134.

[15] Facista A, Nguyen H, Lewis C, Prasad AR, Ramsey L, Zaitlin B, Nfonsam V, Krouse RS, Bernstein H, Payne CM, Stern S, Oatman N, Banerjee B and Bernstein C. Deficient expression of DNA repair enzymes in early progres-

sion to sporadic colon cancer. Genome Integr 2012; 3: 3.
[16] Franklin WA, Gazdar AF, Haney J, Wistuba II, La Rosa FG, Kennedy T, Ritchey DM and Miller YE. Widely dispersed p53 mutation in respiratory epithelium. A novel mechanism for field carcinogenesis. J Clin Invest 1997; 100: 2417-2639.
[17] Heaphy CM, Griffith JK and Bisoffi M. Mammary field cancerization: molecular evidence and clinical importance. Breast Cancer Res Treat 2009; 118: 229-239.
[18] Jones TD, Wang M, Eble JN, MacLennan GT, Lopez-Beltran A, Zhang S, Cocco A and Cheng L. Molecular evidence supporting field effect in urothelial carcinogenesis. Clin Cancer Res 2005; 11: 6512-6519.
[19] Jothy S, Slesak B, Harlozinska A, Lapinska J, Adamiak J and Rabczynski J. Field effect of human colon carcinoma on normal mucosa: relevance of carcinoembryonic antigen expression. Tumour Biol 1996; 17: 58-64.
[20] Kadara H, Fujimoto J, Yoo SY, Maki Y, Gower AC, Kabbout M, Garcia MM, Chow CW, Chu Z, Mendoza G, Shen L, Kalhor N, Hong WK, Moran C, Wang J, Spira A, Coombes KR and Wistuba II. Transcriptomic architecture of the adjacent airway field cancerization in non-small cell lung cancer. J Natl Cancer Inst 2014; 106: dju004.
[21] Lynch SP, Lei X, Hsu L, Meric-Bernstam F, Buchholz TA, Zhang H, Hortobagyi GN, Gonzalez-Angulo AM and Valero V. Breast cancer multifocality and multicentricity and locoregional recurrence. Oncologist 2013; 18: 1167-1173.
[22] Nonn L, Ananthanarayanan V and Gann PH. Evidence for field cancerization of the prostate. Prostate 2009; 69: 1470-1479.
[23] Kuhl S, Voss E, Scherer A, Lusche DF, Wessels D and Soll DR. 4D Tumorigenesis model for quantitating coalescence, quantitating directed cell motility and chemotaxis, identifying unique cell behaviors and testing anti-cancer drugs. In: Hereld D, Jin T, editors. Chemotaxis: Methods and Protocols. Springer; 2015.
[24] Scherer A, Kuhl S, Wessels D, Lusche DF, Hanson B, Ambrose J, Voss E, Fletcher E, Goldman C and Soll DR. A Computer-Assisted 3D Model for Analyzing the Aggregation of Tumorigenic Cells Reveals Specialized Behaviors and Unique Cell Types that Facilitate Aggregate Coalescence. PLoS One 2015; 10: e0118628.
[25] Wessels D, Lusche DF, Kuhl S, Scherer A, Voss E and Soll DR. Quantitative Motion Analysis in Two and Three Dimensions. In: Gavin R, editors. Cytokeleton Methods and Protocols. 3. New York, Heildelberg: Springer; 2015.
[26] Jensen EC. Use of fluorescent probes: their effect on cell biology and limitations. Anat Rec (Hoboken) 2012; 295: 2031-2036.
[27] Sung MH. A Checklist for Successful Quantitative Live Cell Imaging in Systems Biology. Cells 2013; 2: 284-293.
[28] Soule HD, Maloney TM, Wolman SR, Peterson WD Jr, Brenz R, McGrath CM, Russo J, Pauley RJ, Jones RF and Brooks SC. Isolation and characterization of a spontaneously immortalized human breast epithelial cell line, MCF-10. Cancer Res 1990; 50: 6075-6086.
[29] Hendrix MJ, Seftor EA, Seftor RE and Trevor KT. Experimental co-expression of vimentin and keratin intermediate filaments in human breast cancer cells results in phenotypic interconversion and increased invasive behavior. Am J Pathol 1997; 150: 483-495.
[30] Keller PJ, Lin AF, Arendt LM, Klebba I, Jones AD, Rudnick JA, DiMeo TA, Gilmore H, Jefferson DM, Graham RA, Naber SP, Schnitt S and Kuperwasser C. Mapping the cellular and molecular heterogeneity of normal and malignant breast tissues and cultured cell lines. Breast Cancer Res 2010; 12: R87.
[31] Baugher PJ, Krishnamoorthy L, Price JE and Dharmawardhane SF. Rac1 and Rac3 isoform activation is involved in the invasive and metastatic phenotype of human breast cancer cells. Breast Cancer Res 2005; 7: R965-974.
[32] Price JE, Polyzos A, Zhang RD and Daniels LM. Tumorigenicity and metastasis of human breast carcinoma cell lines in nude mice. Cancer Res 1990; 50: 717-721.
[33] Soll D and Voss E. Two and three dimensional computer systems for analyzing how cells crawl. In: Soll D, Wessels D, editors. Motion Analysis of Living Cells. John Wiley, Inc; 1998. pp. 25-52.
[34] Soll DR. The use of computers in understanding how animal cells crawl. Int Rev Cytol 1995; 163: 43-104.
[35] Soll DR, Wessels D, Voss E and Johnson O. Computer-assisted systems for the analysis of amoeboid cell motility. Methods Mol Biol 2001; 161: 45-58.
[36] Wessels D, Kuhl S and Soll DR. Application of 2D and 3D DIAS to motion analysis of live cells in transmission and confocal microscopy imaging. Methods Mol Biol 2006; 346: 261-279.
[37] Wessels D, Kuhl S and Soll DR. 2D and 3D quantitative analysis of cell motility and cytoskeletal dynamics. Methods Mol Biol 2009; 586: 315-335.
[38] Lee GY, Kenny PA, Lee EH and Bissell MJ. Three-dimensional culture models of normal and malignant breast epithelial cells. Nat Methods 2007; 4: 359-365.
[39] Poston T, Wong TT and Heng PA. Multiresolution isosurface extraction with adaptive skeleton climbing. Computer Graphics Forum 1998; 17: 137-147.

[40] Hermann L. Laplacian-isoparametric grid generation scheme. J Engin Mech Div 1976; 102: 749-756.
[41] Soll DR. Computer-assisted three-dimensional reconstruction and motion analysis of living, crawling cells. Comput Med Imaging Graph 1999; 23: 3-14.
[42] Soll DR, Voss E, Johnson O and Wessels D. Three-dimensional reconstruction and motion analysis of living, crawling cells. Scanning 2000; 22: 249-257.
[43] Soll DR, Wessels D, Heid PJ and Voss E. Computer-assisted reconstruction and motion analysis of the three-dimensional cell. ScientificWorldJournal 2003; 3: 827-841.
[44] Wessels D, Vawter-Hugart H, Murray J and Soll DR. Three-dimensional dynamics of pseudopod formation and the regulation of turning during the motility cycle of Dictyostelium. Cell Motil Cytoskel 1994; 27: 1-12.
[45] Maron MJ. Numerical Analysis. New York: Macmillan; 1982.
[46] Lusche DF, Wessels D, Ryerson DE and Soll DR. Nhe1 is essential for potassium but not calcium facilitation of cell motility and the monovalent cation requirement for chemotactic orientation in Dictyostelium discoideum. Eukaryot Cell 2011; 10: 320-331.
[47] Sarria S, Nordeen S and Evans R. Regulated expression of vimentin cDNA in cells in the presence and absence of a preexisting vimentin filament network. J Cell Biol 1990; 111: 553-565.
[48] Gunning P, Leavitt J, Muscat G, Ng SY and Kedes L. A human beta-actin expression vector system directs high-level accumulation of antisense transcripts. Proc Natl Acad Sci U S A 1987; 84: 4831-4835.
[49] Scherer A, Kuhl S, Wessels D, Lusche DF, Raisley B and Soll DR. Ca^{2+} chemotaxis in Dictyostelium discoideum. J Cell Sci 2010; 123: 3756-3767.
[50] Wessels D, Lusche DF, Steimle PA, Scherer A, Kuhl S, Wood K, Hanson B, Egelhoff TT and Soll DR. Myosin heavy chain kinases play essential roles in Ca^{2+}, but not cAMP, chemotaxis and the natural aggregation of Dictyostelium discoideum. J Cell Sci 2012; 125: 4934-4944.
[51] Doyle AD, Petrie RJ, Kutys ML and Yamada KM. Dimensions in cell migration. Current Opinion in Cell Biology 2013; 25: 642-649.
[52] Soll DR, Wessels D, Kuhl S and Lusche DF. How a cell crawls and the role of cortical myosin II. Eukaryot Cell 2009; 8: 1381-1396.
[53] Soule HD, Vazguez J, Long A, Albert S and Brennan M. A human cell line from a pleural effusion derived from a breast carcinoma. J Natl Cancer Inst 1973; 51: 1409-1416.
[54] Gilles C, Polette M, Zahm JM, Tournier JM, Volders L, Foidart JM and Birembaut P. Vimentin contributes to human mammary epithelial cell migration. J Cell Sci 1999; 112: 4615-4625.
[55] Hendrix MJ, Seftor EA, Chu YW, Trevor KT and Seftor RE. Role of intermediate filaments in migration, invasion and metastasis. Cancer Metastasis Rev 1996; 15: 507-525.
[56] Zhao Y, Yan Q, Long X, Chen X and Wang Y. Vimentin affects the mobility and invasiveness of prostate cancer cells. Cell Biochem Funct 2008; 26: 571-577.
[57] Midwood KS, Williams LV and Schwarzbauer JE. Tissue repair and the dynamics of the extracellular matrix. Int J Biochem Cell Biol 2004; 36: 1031-1037.
[58] Hardin J. The role of secondary mesenchyme cells during sea urchin gastrulation studied by laser ablation. Development 1988; 103: 317-324.
[59] Shabbir SH, Cleland MM, Goldman RD and Mrksich M. Geometric control of vimentin intermediate filaments. Biomaterials 2014; 35: 1359-1366.
[60] Hendrix MJ, Seftor EA, Chu YW, Seftor RE, Nagle RB, McDaniel KM, Leong SP, Yohem KH, Leibovitz AM, Meyskens FL Jr, Conaway DH, Welch DR, Liotta LA and Stetler-Stevenson W. Coexpression of vimentin and keratins by human melanoma tumor cells: correlation with invasive and metastatic potential. J Natl Cancer Inst 1992; 84: 165-174.
[61] Tripathi M, Billet S and Bhowmick NA. Understanding the role of stromal fibroblasts in cancer progression. Cell Adh Migr 2012; 6: 231-235.

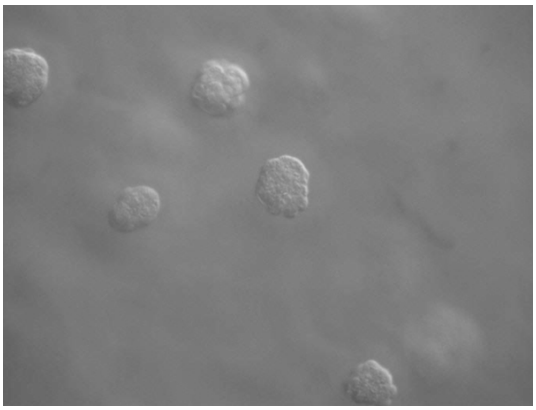

Supplementary Movie 1. Non-coalescing MCF-7. Cells from the weakly tumorigenic cell line MCF-7 divide to form islands of cells (primary aggregates) that do not undergo coalescence, seeded in 3D Matrigel. Movie is a series of DIC images from a single plane acquired at 30 minute intervals over a period of 70 hours.

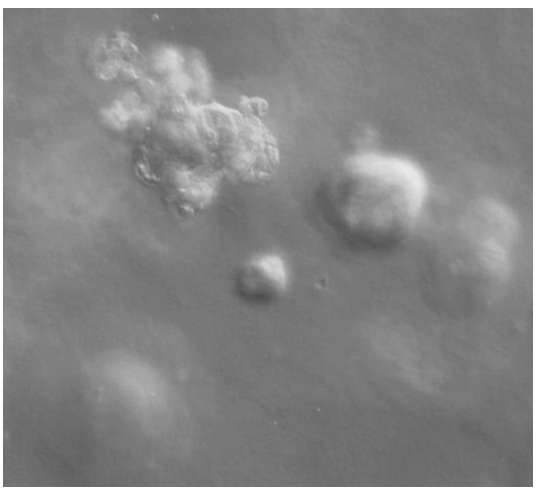

Supplementary Movie 2. Coalescing MoVi-10. Cells from the tumorigenic cell line MoVi-10´ undergo rapid coalescence when embedded in 3D Matrigel matrix. Movie is a time series of DIC images at a single plane, acquired at 30 minute intervals over a period of 70 hours.

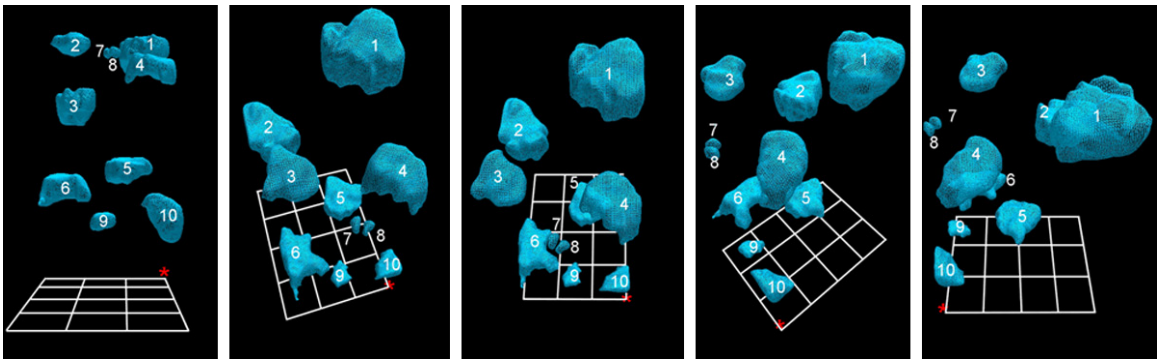

Supplementary Figure 1. Rotations of 3D reconstructions at the 50 hour time point in a preparation of aggregates containing 90% MCF-7 and 10% MoVi-10´ cells (**Figure 9**) demonstrates 10 independent aggregates and their relative positions prior to the onset of coalescence. The asterisk on the right rear corner of the grid in panel one is a reference point for rotation of the grid.